Inorganic Chemistry

Article

pubs.acs.org/IC

A-Site-Ordered Perovskite $MnCu_3V_4O_{12}$ with a 12-Coordinated Manganese(II)

Yasuhide Akizuki,[†] Ikuya Yamada,*[,‡,§] Koji Fujita,*[,†] Norimasa Nishiyama,[§,∥,⊥] Tetuo Irifune,[∥] Takeshi Yajima,[#] Hiroshi Kageyama,[#] and Katsuhisa Tanaka[†]

[†]Department of Material Chemistry, Graduate School of Engineering, Kyoto University, Katsura, Nishikyo-ku, Kyoto 615-8510, Japan

[‡]Nanoscience and Nanotechnology Research Center, Osaka Prefecture University, 1-2 Gakuen-cho, Naka-ku, Sakai, Osaka 599-8531, Japan

[§]JST-PRESTO, 4-1-8 Honcho Kawaguchi, Saitama 332-0012, Japan

[∥]Geodynamics Research Center, Ehime University, 2-5 Bunkyo-cho, Matsuyama, Ehime 790-8577, Japan

[⊥]Deutsches Elektronen Synchrotron, 22607 Hamburg, Germany

[#]Department of Energy and Hydrocarbon Chemistry, Graduate School of Engineering, Kyoto University, Katsura, Nishikyo-ku, Kyoto 615-8510, Japan

Supporting Information

ABSTRACT: A novel cubic perovskite $MnCu_3V_4O_{12}$ has been synthesized at a high pressure and high temperature of 12 GPa and 1373 K. This compound crystallizes in the *A*-site-ordered perovskite structure (space group $Im\bar{3}$) with lattice constant a = 7.26684(10) Å at room temperature. The most notable feature of this compound lies in the fact that the Mn^{2+} ion is surrounded by 12 equidistant oxide ions to form a regular icosahedron; the situation of Mn^{2+} is unprecedented for the crystal chemistry of an oxide. An anomalously large atomic displacement parameter U_{iso}= 0.0222(8) Å^2 is found for Mn^{2+} at room temperature, indicating that the thermal oscillation of the small Mn^{2+} ion in a large icosahedron is fairly active. Magnetic susceptibility and electric resistivity measurements reveal that 3d electrons of Mn^{2+} ions are mainly localized, while 3d electrons in Cu^{2+} and V^{4+} ions are delocalized and contribute to the metallic conduction.

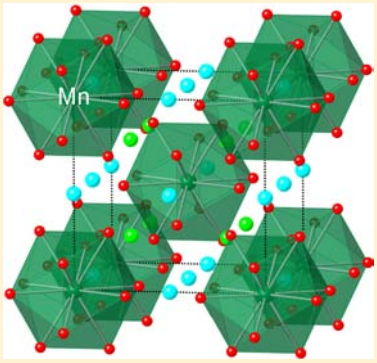

INTRODUCTION

Transition-metal compounds with perovskite and its related structures have attracted much attention because of a large variety of physical properties and their promising technological applications. In general, the ABO_3 perovskite structure becomes unstable when 3d transition-metal ions with small ionic radii are incorporated into the *A* site so that intriguing magnetic and electrical properties are induced through the *A*−*A* and/or *A*−*B* interactions, and instead, other crystal structures such as ilmenite-type and lithium niobate-type come to be stabilized.[1] Some of the ilmenite-type $A^{2+}Ti^{4+}O_3$ compounds, like $MnTiO_3$ and $FeTiO_3$, are transformed to perovskite-type structure under high pressure, but the perovskite phase is unquenchable to ambient pressure, and the resultant compounds crystallize in lithium niobate-type structure.[2,3] In the case of $A^{2+}V^{4+}O_3$ compounds, those with a 3d transition metal on the *A* site cannot be synthesized at ambient pressure, although some compounds like $MnVO_3$, $CoVO_3$, and $CuVO_3$ are stabilized at high pressure and can be quenched to ambient pressure: While $CoVO_3$ and $CuVO_3$ crystallize in the ilmenite-type structure,[4,5] $MnVO_3$ adopts either the ilmenite- or the perovskite-type phase, depending on the synthesis condition.[6] The pressure-induced perovskite $MnVO_3$ is a rare example of a perovskite compound in which the *A* site is entirely occupied by small 3d transition-metal ions. Note that there are a few perovskites with full occupancy of the *A* position by Mn^{2+} accompanied by a notable magnitude of BO_6 octahedral tilt that heavily distorts the cuboctahedrally coordinated *A* sites and thus reduces the coordination number of Mn^{2+} down to 8.[6−8]

Partial occupancy of the *A* sites by 3d transition metals is, nevertheless, possible in a unique class of *A*-site-ordered perovskites $A'A''_3B_4O_{12}$, in which one-quarter of the *A* sites (=*A*′ site), surrounded by 12 O^{2-} ions forming a regular icosahedral configuration, is generally filled with relatively large cations, such as alkali metal, alkaline-earth metal, and lanthanide ions. The remaining three-quarters of the *A* sites (=*A*″ site) are occupied by 3d transition metals, which forces the BO_6 octahedra to tilt in order to stabilize the pseudosquare $A''O_4$ configuration (see Figure 1c). The square-coordinated *A*″ sites tend to be stabilized by residence of Jahn−Teller active ions like Cu^{2+} and Mn^{3+} ions.[9−13] Due to the 1:3 type ordering of *A*′ and *A*″ cations, many compounds in this family crystallize

Received: July 20, 2013
Published: September 12, 2013

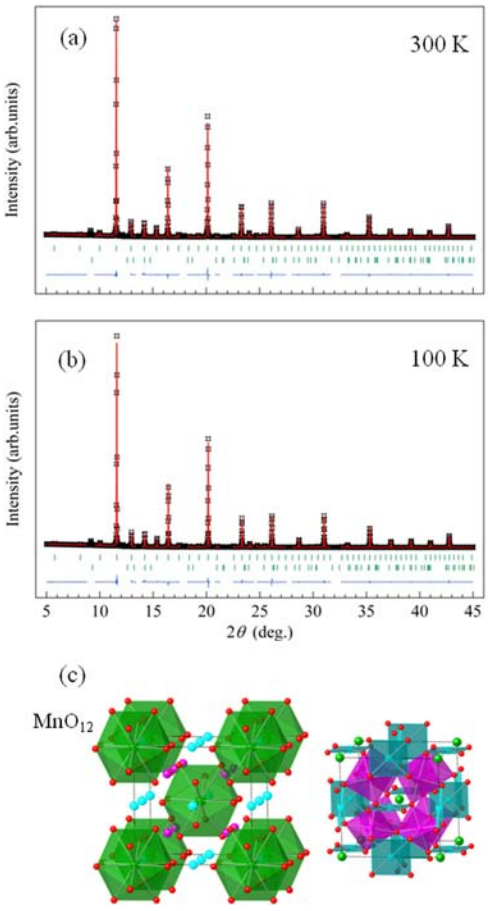

Figure 1. Rietveld refinement of synchrotron powder X-ray diffraction pattern (λ = 0.51897 Å) for $MnCu_3V_4O_{12}$ collected at 300 (a) and 100 K (b), showing the observed (crosses), calculated (solid line), and difference (bottom line) profiles. Upper and lower ticks represent the Bragg reflection positions of $MnCu_3V_4O_{12}$ and VO_2, respectively. (c) Refined crystal structure of $MnCu_3V_4O_{12}$ with MnO_{12} icosahedral units (left) and that with superimposed CuO_4 planes and VO_6 octahedral units (right).

in a enlarged cubic $2a_p \times 2a_p \times 2a_p$ unit cell (space group $Im\bar{3}$) relative to its archetype with a lattice parameter a_p.

Despite the fact that the numerous members of the $A'A''_3B_4O_{12}$ perovskite family have been extensively studied over decades,[9−22] there have been no compounds where 3d transition metals are accommodated in the icosahedrally coordinated A' sites while keeping the cubic symmetry. In the present study, we succeeded in synthesizing $MnCu_3V_4O_{12}$, a structural feature of which is full occupation of the A sites by 3d transition metals in the 1:3 type ordering, using high-pressure and high-temperature treatment. This is the first observation that a small ion such as Mn^{2+} occupies a large cage composed of 12 equidistant O^{2-} ions to form a regular icosahedron. An additional interesting feature is that the small Mn^{2+} ion has an anomalously large atomic displacement parameter at room temperature. We also show that this compound is a metallic oxide in which the 3d electrons in Cu^{2+} and V^{4+} ions are itinerant and the Mn^{2+} spins are mainly localized.

EXPERIMENTAL SECTION

Polycrystalline $MnCu_3V_4O_{12}$ samples were synthesized by solid-state reaction under high pressure at elevated temperature. Reagent-grade MnO (99.9%, Kojundo Chemicals), CuO (99.9%, Mitsuwa Chemicals), and VO_2 (99.9%, Kojundo Chemicals) were employed as starting materials. After appropriate amounts of the starting materials were mixed thoroughly, the mixture was charged into a platinum capsule and put into a high-pressure cell. The high-pressure and high-temperature treatment was performed at 12 GPa and 1373 K using the Kawai-type high-pressure apparatus at the Geodynamics Research Center, Ehime University. After being treated for 20 min, the temperature was quickly cooled to room temperature followed by slow release of the pressure.

The powder X-ray diffraction (XRD) pattern was initially recorded at room temperature on a Rigaku RINT-2500 diffractometer with Cu Kα radiation (λ = 1.5406 Å) to identify the crystalline phase of products. For structural refinement, the synchrotron XRD pattern (SXRD) was collected with a Debye−Scherrer camera installed in the BL02B2 beamline at SPring-8. The wavelength of the incident beam was 0.51897 Å, which was calibrated by the lattice constant of standard CeO_2 powders. Diffraction data were collected at several temperatures between 100 and 400 K in the 2θ range from 0° to 75° with a step interval of 0.01°. The RIETAN-FP program[23] was used to refine the structural parameters by the Rietveld method.

Magnetic susceptibility measurements were performed over the temperature range of 5−300 K using a Quantum Design MPMS-XL magnetometer under zero-field-cooling (ZFC) and field-cooling (FC) conditions employing an external magnetic field of 1000 Oe. Electric resistivity and specific heat were measured between 2 and 250 K utilizing a Quantum Design PPMS in zero magnetic fields. Resistance measurements were carried out for the as-synthesized, fully dense disk using a four-probe method. Silver paste was used to get good electrical contact between Au wires and the bulk sample. The heat-capacity measurement was performed using a heat pulse relaxation technique. The sample was mounted on a thin alumina plate with grease for better thermal contact.

RESULTS AND DISCUSSION

The laboratory XRD pattern of the sample collected at room temperature reveals a cubic perovskite structure with superstructure peaks associated with the A-site cationic ordering. Once quenched, the perovskite phase is metastable at ambient pressure and does not show decomposition at room temperature after 6 months at least.

Figure 1a shows the room-temperature SXRD pattern of $MnCu_3V_4O_{12}$ and the result of analysis by the Rietveld method. Rietveld refinement of SXRD data was carried out in the space group of $Im\bar{3}$ (No. 204) using the $CaCu_3V_4O_{12}$ structure as the starting model. In the structural model, Mn, Cu, V, and O atoms were placed at 2a (0, 0, 0), 6b (0, 1/2, 1/2), 8c (1/4, 1/4, 1/4), and 24g (x, y, 0) sites, respectively.[24] This model could result in a good fit (R_{wp} = 5.278%). A few weak diffraction peaks from VO_2 ($P4_2/nmn$) and unidentified phases were detected, but the amount of these impurity phases was assumed to be a few wt %. In this model, however, the atomic displacement parameter of Mn is as large as U_{iso} = 0.0222(8) Å^2, although the U_{iso} values of the Cu and V atoms are reasonably small (U_{iso} < 0.005 Å^2). Such a large U_{iso} value is ascribed to either static disorder or dynamic atomic vibrations. For the static disorder we first checked the possibility of Mn deficiency at the 2a positions (A' sites), but the site occupancy did not deviate from the full fraction during the refinements. Then, the Mn displacive disorder that the Mn atom moved out from the ideal 2a to more general sites was explored using several split-atom models. We considered possible three kinds of Mn displacements along ⟨100⟩, ⟨110⟩, and ⟨111⟩ directions, modeled by occupancy of 12d (x, 0, 0), 24g (x, x, 0), and 16f (x, x, x) positions, respectively. Table 1 compares the R factors and U_{iso} value obtained for the ideal-position model with those for the three displacive models. The involvement of displacive

dx.doi.org/10.1021/ic401855j | Inorg. Chem. 2013, 52, 11538−11543

Table 1. *R* Factors, Goodness of Fit, and Atomic Displacement Parameter (U_{iso}) of Mn Atoms Obtained by Refining the Room-Temperature SXRD Data with the Structural Model with Mn on the Ideal (2*a*) Position and Those with Mn Displacement Along ⟨100⟩, ⟨110⟩, and ⟨111⟩ Directions

	structural model			
	ideal-position model	⟨100⟩ model	⟨110⟩ model	⟨111⟩ model
R_{wp} (%)	5.278	5.276	5.272	5.272
R_B (%)	3.255	3.278	3.265	3.297
goodness of fit	0.8170	0.8167	0.8162	0.8161
$100 \times U_{iso}$ (Å^2)	2.22(8)	0.7(6)	0.3(5)	0.5(5)

disorder in refinement brings about the smaller U_{iso} values compared to the ideal-position model but with no improvement in *R* factors, which implies an insignificant contribution from the off-center Mn displacement.

The crystal structure of $MnCu_3V_4O_{12}$ refined by the ideal-position model is illustrated in Figure 1c, and structural parameters as well as selected bond lengths and angles obtained by Rietveld analysis are summarized in Table 2. The lattice

Table 2. Refined Structure Parameters, Selected Bond Lengths, and Bond Angles at 100 and 300 K for $MnCu_3V_4O_{12}$[a]

	300 K	100 K
a (Å)	7.26684(10)	7.25469(12)
x (O)	0.3028(3)	0.3025(4)
y (O)	0.1822(3)	0.1821(4)
$100 \times U_{iso}$ (Mn) (Å^2)	2.22(8)	1.15(8)
$100 \times U_{iso}$ (Cu) (Å^2)	0.42(3)	0.26(3)
$100 \times U_{iso}$ (V) (Å^2)	0.37(2)	0.19(2)
$100 \times U_{iso}$ (O) (Å^2)	0.27(5)	0.09(5)
Mn−O (Å)	2.568(3)	2.562(3)
Cu−O (Å)	1.951(2)	1.949(2)
Cu−O (Å)	2.718(3)	2.715(3)
V−O (Å)	1.9210(7)	1.9177(8)
V−O−V (deg)	142.06(11)	142.09(13)
R_{wp} (%)	5.278	6.193
R_B (%)	3.255	3.771
goodness of fit	0.8170	0.9633

[a]Space group: $Im\bar{3}$ (No. 204). Atomic sites: Mn 2*a* (0, 0, 0), Cu 6*b* (0, 1/2, 1/2), V 8*c* (1/4, 1/4, 1/4), O 24*g* (*x*, *y*, 0). Site occupancy for all atoms was fixed to 1.

constant *a* of $MnCu_3V_4O_{12}$ at room temperature (7.267 Å) is almost identical to that of $CaCu_3V_4O_{12}$ (a = 7.281 Å),[24] and the metal−oxygen bond lengths (Mn/Ca−O, Cu−O, and V−O) and V−O−V bond angle are not very different between $MnCu_3V_4O_{12}$ and $CaCu_3V_4O_{12}$. This is in sharp contrast to the observed behavior in a series of AVO_3 perovskites (A = Sr, Ca, and Mn) where the reduced size of the A^{2+} cation from Sr to Mn is accommodated by a concomitant decrease in the V−O−V angle due to the tilting of VO_6 octahedra; the V−O−V angle for AVO_3 is about 180°, 161°, and 144° for A = Sr,[25] Ca,[26] and Mn,[7] respectively. For $MnVO_3$, the considerable tilting of VO_6 octahedra generates three types of Mn−O bond lengths: 4 short (2.2 Å), 4 medium (2.4−2.6 Å), and 4 long (3.1−3.4 Å) Mn−O bonds. Since the Mn−O bond length over 3.0 Å is longer than the separation of the nearest neighboring Mn−V bond (2.957 Å), the coordination number of Mn^{2+} is regarded as 8-fold in $MnVO_3$. As a result of the severe octahedral tilting, Mn^{2+} ions fit into the cavity of the distorted AO_8 polyhedra and the bond valence sums (BVS)[27] calculated from the bond lengths are +2.02 and +3.98 for Mn and V, respectively,[28] in agreement with a simple ionic model ($Mn^{2+}V^{4+}O_3$). For $MnCu_3V_4O_{12}$, on the other hand, the BVS calculated from structural data is +1.47, +2.16, and +4.14 for Mn, Cu, and V, respectively.[29] While the BVS of Cu and V is close to the values expected from the ionic model ($Mn^{2+}Cu^{2+}{}_3V^{4+}{}_4O_{12}$), the Mn ions are fairly underbonded, reflecting their incorporation into the oversized $A'O_{12}$ icosahedral cage. This is also supported by the fact that the volume of the regular MnO_{12} icosahedra in $MnCu_3V_4O_{12}$ (42.9 Å^3) is much larger than that of the distorted MnO_8 polyhedra in $MnVO_3$ (21.4 Å^3).[30] Thus, the icosahedral cage in $MnCu_3V_4O_{12}$ should be large enough for Mn ion to oscillate thermally, in contrast to other perovskites with Mn^{2+} occupying the A sites.[7,8,22]

In order to further examine the behavior of thermal parameters of $MnCu_3V_4O_{12}$, we measured temperature-variable SXRD and estimated the U_{iso} values of the Mn, Cu, V, and O atoms at several temperatures down to 100 K. A representative SXRD pattern at 100 K is shown in Figure 1b, together with the result of Rietveld analysis. Rietveld refinement with the ideal-position model converged to R_{wp} = 6.193% (see also Table 2), indicating that there is no structural transition down to 100 K. The temperature variation of U_{iso} is displayed in Figure 2. One

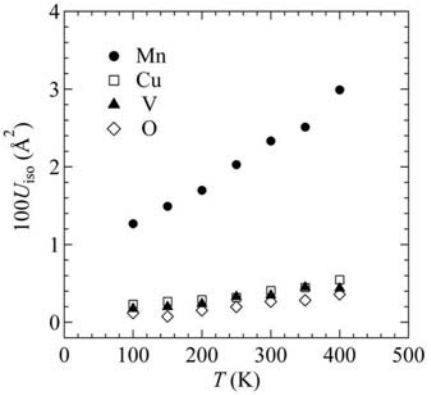

Figure 2. Temperature dependence of U_{iso} for Mn, Cu, V, and O in $MnCu_3V_4O_{12}$.

can see a general tendency for the U_{iso} value to decrease with decreasing temperature. Remarkably, the U_{iso} value for the Mn atom shows stronger temperature dependence than those for Cu and V atoms. In addition, the U_{iso} value for Mn remains enhanced even at 100 K as compared to those for Cu and V atoms. These results indicate that Mn ions in $MnCu_3V_4O_{12}$ are weakly bound in the icosahedral cage. Such behavior of U_{iso} has been also observed for cage-structured compounds such as filled skutterudites,[31] clathrates,[32] and β-pyrochlore oxides,[33] where guest ions are endohedrally accommodated in polyhedral cages and therefore the guest−host interaction is weak. Thus, it is reasonable to conclude that the vibration amplitude of the Mn atom inside the icosahedral cage is very large at room temperature and thus contributes significantly to the thermal parameter.

Here, it should be noted that owing to their network composed of rigid planar $A''O_4$ and heavily tilted octahedral BO_6 units, $A'A''{}_3B_4O_{12}$ compounds sometimes exhibit a

dx.doi.org/10.1021/ic401855j | Inorg. Chem. 2013, 52, 11538−11543

deviation from the general trend that the A' sites are occupied by relatively large cations. For example, the A' sites tolerate occupation by the smallest lanthanide ion (e.g., Lu-$Cu_3Mn_4O_{12}$)[18] and even a full vacancy (e.g., $\square Cu_3Ti_2Ta_2O_{12}$)[11] while leaving its icosahedral configuration intact. The capability for the icosahedral A' site to accommodate cationic vacancies and a wide range of cations of different sizes is a key factor to achieve the unprecedented coordination geometry of Mn^{2+} in $MnCu_3V_4O_{12}$.

To obtain information about the electronic states of transition-metal ions in $MnCu_3V_4O_{12}$, we characterized its magnetic and electrical properties. Figure 3 shows the

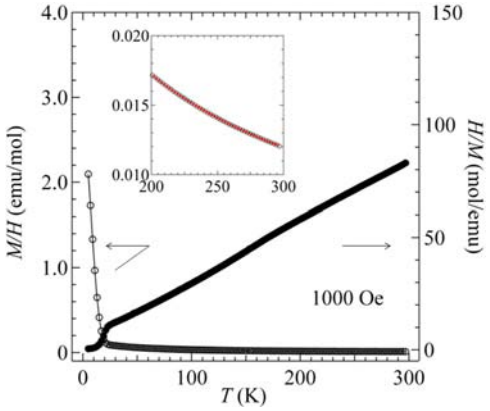

Figure 3. Temperature dependence of the magnetic susceptibility χ ($=M/H$) of $MnCu_3V_4O_{12}$ measured at an external field of 1000 Oe under a field-cooled condition (open circles). Relationship of χ^{-1} versus T is also indicated by closed circles. (Inset) Fit of a modified Curie–Weiss law to the $\chi(T)$ data between 199 and 285 K.

temperature dependence of magnetic susceptibility $\chi(T)$ and its reciprocal $\chi^{-1}(T)$ for $MnCu_3V_4O_{12}$. No significant difference in $\chi(T)$ was seen between FC and ZFC conditions. A nearly linear relation is observed for the $\chi^{-1}(T)$ curve in the high-temperature range between 200 and 300 K, showing paramagnetic Curie–Weiss behavior, which is in contrast to the temperature-independent behavior due to the Pauli paramagnetism in the isostructural $ACu_3V_4O_{12}$ (A = Na, Ca, and Y).[34] Below 200 K, $\chi(T)$ starts to deviate from the Curie–Weiss law and steeply increases at around 20 K. The temperature dependence of electric resistivity (Figure 4) shows a metallic conductivity ($d\rho/dT > 0$) above about 20 K. Between 20 and 140 K, $\rho(T)$ data follow a T^2 dependence (see the inset of Figure 4), being characterized as Fermi-liquid-like behavior. We thus analyzed the $\chi(T)$ data in the high-temperature range using a modified Curie–Weiss law: $\chi(T) = \chi_0 + C/(T - \Theta_W)$, where χ_0 denotes the temperature-independent term, C the Curie constant, and Θ_W the Weiss temperature. $\chi_0 = 9.65(5) \times 10^{-4}$ emu/mol determined by this analysis is of the same order of magnitude as the Pauli paramagnetic term for the isostructural $ACu_3V_4O_{12}$ (A = Na, Ca, and Y) where the electrons in both Cu^{2+} and V^{4+} sites are delocalized to supply itinerant electrons.[34] Analysis also yields $C = 3.40(3)$ emu K^{-1} mol^{-1} and $\Theta_W = -9.5(1.1)$ K, showing very weak antiferromagnetic interactions. Indeed, the temperature dependence of specific heat shows no λ-type anomalies down to 2 K (Figure 5), indicating the absence of long-range magnetic order. Considering the fact that $ACu_3V_4O_{12}$ (A = Na, Ca, and Y) compounds with Cu and V 3d itinerant electrons have no T-dependent Curie-type contribution (except for the

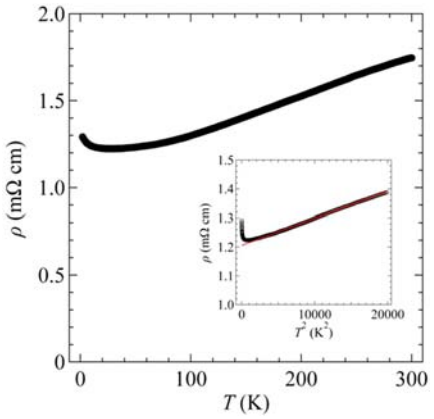

Figure 4. Temperature dependence of electric resistivity ρ of $MnCu_3V_4O_{12}$. (Inset) Low-temperature part of ρ on a T^2 scale (open circles). T^2 dependence of ρ is indicated by the solid line of the inset.

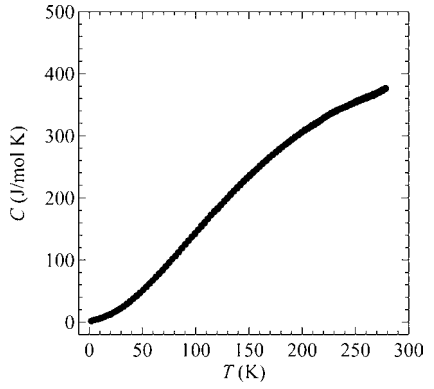

Figure 5. Temperature dependence of specific heat C of $MnCu_3V_4O_{12}$.

impurities) in their $\chi(T)$ data,[34] it is naturally considered that in $MnCu_3V_4O_{12}$ a majority of Mn (A' site) 3d electrons are localized and the Cu (A'' site) and V (B site) 3d electrons are delocalized to cause the metallic behavior. The effective magnetic moment (5.21 μ_B/Mn) is slightly smaller than the spin-only value for Mn^{2+} (S = 5/2, 5.916 μ_B), presumably due to the itinerant character of some Mn electrons. The overall results of the magnetic susceptibility and transport data for $MnCu_3V_4O_{12}$ demonstrate the presence of two types of 3d electrons, i.e., localized and delocalized electrons. A similar behavior is observed for a perovskite $MnVO_3$ with an effective magnetic moment of 5.80 μ_B, in which Mn (A site) $3d^5$ electrons are localized and V (B site) $3d^1$ electrons are itinerant.[7] In $MnVO_3$, antiferromagnetic interactions are dominant ($\Theta_W = -154$K) and incommensurate antiferromagnetic order occurs below 50 K as a result of Mn–O–Mn superexchange and Ruderman–Kittel–Kasuya–Yoshida couplings.[7] In $MnCu_3V_4O_{12}$, on the other hand, the Cu^{2+} ion is located between the neighboring Mn^{2+} ions to form Mn–O–Cu–O–Mn paths. Given the delocalized Cu $3d^9$ electrons, a direct exchange interaction between the neighboring Mn^{2+} ions or an indirect exchange interaction mediated by carriers should dominate the magnetic structure, rather than the Mn–O–Cu superexchange interaction. Due to the longer distance between the neighboring Mn ions in $MnCu_3V_4O_{12}$ compared to $MnVO_3$, nevertheless, the magnetic interaction becomes weaker in the former compound, as signified by $\Theta_W \approx -10$ K.

dx.doi.org/10.1021/ic401855j | Inorg. Chem. 2013, 52, 11538–11543

Although the present study focuses on the unusual coordination geometry of Mn^{2+}, comparison of the crystal structure between *A*-site-ordered perovskites $A'A''_3B_4O_{12}$ and filled skutterudites RM_4X_{12} (*R* = rare-earth metals, *M* = Fe, Ru, and Os, and *X* = P, As, and Sb) provides an opportunity to consider a structure−property relation that is unfamiliar to perovskite oxides. Both $A'A''_3B_4O_{12}$ and RM_4X_{12} compounds have the same space group ($Im\bar{3}$), and the crystallographic sites of *A*′, *B*, and O atoms in the former are identical with those of *R*, *M*, and *X* atoms in the latter, respectively. For filled skutterudites, it is well known that *R* ions are weakly bound in the oversized atomic cage formed by the *X*-icosahedron and tend to exhibit exceptionally large U_{iso} values,[31,35,36] corresponding to thermally activated rattling.[37−40] In the case of $PrOs_4Sb_{12}$ and $NdOs_4Sb_{12}$ compounds, the rattling effect has been observed by ultrasonic experiment[39,40] and Pr and Nd ions have large U_{iso} values of 0.0363 and 0.0482 Å^2 at 300 K, respectively.[41,42] Similarly, the large-amplitude thermal oscillation at room temperature, which is associated with a rattling motion, has been observed for other cage compounds such as clathrates and *β*-pyrochlore oxides, for example, U_{iso}= 0.033 Å^2 for Ba in clathrate compound $Ba_8Ge_{16}Si_{30}$,[43] and U_{iso}= 0.0735, 0.043, and 0.025 Å^2 for *A* = K, Rb, and Cs in *β*-pyrochlore oxides AOs_2O_6, respectively.[33] Regarding the thermal oscillation of the small cation in the oversized cage, there is an obvious similarity between $MnCu_3V_4O_{12}$ and cage compounds. Further studies should be performed on $MnCu_3V_4O_{12}$ to clarify the relation between thermal oscillation and rattling motion.

SUMMARY

We succeeded in synthesizing the *A*-site-ordered perovskite $MnCu_3V_4O_{12}$ using a solid-state reaction under 12 GPa and 1373 K and performed SXRD, magnetic susceptibility, electric resistivity, and specific heat studies. Rietveld refinement of SXRD data reveals that the compound has a cubic perovskite structure with Mn^{2+} occupying a 12-coordinated site to form a regular icosahedron with 12 equivalent Mn−O bonds. To our knowledge, the residence of Mn^{2+} in such a highly symmetrical and large cage of icosahedral environment has been never obtained so far. The Mn^{2+} ion in $MnCu_3V_4O_{12}$ exhibits a large atomic displacement parameter at room temperature, suggesting the fairly active thermal oscillation of Mn^{2+} in the oversized cage. From the magnetic susceptibility and electric resistivity measurements it is found that the Mn 3d electrons are mainly localized while the Cu and V 3d electrons possess the itinerant feature giving rise to metallic conduction.

ASSOCIATED CONTENT

Supporting Information

Crystallographic data (CIF) of $MnCu_3V_4O_{12}$. This material is available free of charge via the Internet at http://pubs.acs.org.

AUTHOR INFORMATION

Corresponding Author

* E-mail: i-yamada@21c.osakafu-u.ac.jp (I.Y.); fujita@dipole7.kuic.kyoto-u.ac.jp (K.F.).

Notes

The authors declare no competing financial interest.

ACKNOWLEDGMENTS

Synchrotron radiation experiments were performed at the SPring-8 with the approval of the Japan Synchrotron Radiation Research Institute (Proposal Nos. 2011A1641, 2012A1677, and 2012A1554). We thank J. Kim and N. Tsuji for the SXRD experiments at the BL02B2 beamline of SPring-8. This work was partly supported by the Global COE Program "International Center for Integrated Research and Advanced Education in Material Science".

REFERENCES

(1) Navrotsky, A. *Chem. Mater.* **1998**, *10*, 2787.
(2) Wu, X.; Qin, S.; Dubrovinsky, L. *Geosci. Front.*. **2011**, *2* (1), 107.
(3) Ming, L. C.; Kim, Y. Ho.; Uchida, T.; Wang, Y.; Rivers, M. *Am. Mineral.* **2006**, *91*, 120.
(4) Chamberland, B. L. *J. Solid State Chem.* **1970**, *1*, 138.
(5) Chamberland, B. L. *J. Solid State Chem.* **1970**, *2*, 521.
(6) Syono, Y.; Akimoto, S.; Endoh, Y. *J. Phys. Chem. Solids* **1971**, *32*, 243.
(7) Markkula, M.; Arevalo-Lopez, A. M.; Kusmartseva, A.; Rodgers, J. A.; Ritter, C.; Wu, H.; Attfield, J. P. *Phys. Rev. B* **2011**, *84*, 094450.
(8) Tyutyunnik, A. P.; Bazuev, G. V.; Kuznetsov, M. V.; Zainulin, Y. G. *Mater. Res. Bull.* **2011**, *46*, 1247.
(9) Bochu, B.; Chenavas, J.; Joubert, J. C.; Marezio, M. *J. Solid State Chem.* **1974**, *11*, 83.
(10) Chenavas, J.; Joubert, J. C.; Marezio, M.; Bochu, B. *J. Solid State Chem.* **1975**, *14*, 25.
(11) Lebeau, M.; Bochu, B.; Joubert, J. C.; Chenavas, J. *J. Solid State Chem.* **1980**, *33*, 257.
(12) Subramanian, M. A.; Sleight, A. W. *Solid State Sci.* **2002**, *4*, 347.
(13) Vasil'ev, A. N.; Volkova, O. S. *Low Temp. Phys.* **2007**, *33*, 895.
(14) Ramirez, A. P.; Subramanian, M. A.; Gardel, M.; Blumberg, G.; Li, D.; Vogt, T.; Shapiro, S. M. *Solid State Commun.* **2000**, *115*, 217.
(15) Zeng, Z.; Greenblatt, M.; Subramanian, M. A.; Croft, M. *Phys. Rev. Lett.* **1999**, *82*, 3164.
(16) Alonso, J. A.; Sánchez-Benítez, J.; Andrés, A. De.; Martínez-Lope, M. J.; Casais, M. T.; Martínez, J. L. *Appl. Phys. Lett.* **2003**, *83*, 2623.
(17) Sánchez-Benítez, J.; Alonso, J. A.; Martínez-Lope, M. J.; Andrés, A. De.; Fernández-Díaz, M. T. *Inorg. Chem.* **2010**, *49*, 5679.
(18) Kobayashi, W.; Terasaki, I.; Takeya, J.; Tsukada, I.; Ando, Y. *J. Phys. Soc. Jpn.* **2004**, *73*, 2373.
(19) Ramirez, A. P.; Lawes, G.; Li, D.; Subramanian, M. A. *Solid State Commun.* **2004**, *131*, 251.
(20) Long, Y. W.; Hayashi, N.; Saito, T.; Azuma, M.; Muranaka, S.; Shimakawa, Y. *Nature* **2009**, *458*, 60.
(21) Yamada, I.; Tsuchida, K.; Ohgushi, K.; Hayashi, N.; Kim, J.; Tsuji, N.; Takahashi, R.; Matsushita, M.; Nishiyama, N.; Inoue, T.; Irufune, T.; Kato, K.; Takata, M.; Takano, M. *Angew. Chem., Int. Ed.* **2011**, *50*, 6579.
(22) Ovsyannikov, S. V.; Abakumov, A. M.; Tsirlin, A. A.; Schnelle, W.; Egoavil, R.; Verbeeck, J.; Van Tendeloo, G.; Glazyrin, K. V.; Hanfland, M.; Dubrovinsky, L. *Angew. Chem., Int. Ed.* **2013**, *52*, 1494.
(23) Izumi, F.; Momma, K. *Solid State Phenom.* **2007**, *130*, 15.
(24) Kadyrova, N. I.; Tyutyunnik, A. P.; Zubkov, V. G.; Zakharova, G. S.; Volkov, V. L.; Dyachkova, T. V.; Zainulin, Y. G. *Russ. J. Inorg. Chem.* **2003**, *48*, 1785.
(25) Lan, Y. C.; He, Chwn, M. *J. Alloys Compd.* **2003**, *354*, 95.
(26) Garcia-Jaca, J.; Ignacio, J.; Larrmendi, R.; Insausti, M.; Isabel Arriortua, M.; Rojo, T. *J. Mater. Chem.* **1995**, *5*, 1995.
(27) Brown, I. D.; Altermatt, D. *Acta Crystallogr., Sect B: Struct. Sci.* **1985**, *B41*, 244.
(28) BVS of Mn and V of $MnVO_3$ was calculated from the bond lengths reported in ref 7 using the following parameters: b_0 = 0.37 for all and r_0 = 1.790 and 1.784 for Mn and V, respectively.
(29) BVS of $MnCu_3V_4O_{12}$ was calculated from the structural data in Table 2 using the following parameters: b_0 = 0.37 for all and r_0 = 1.790, 1.679 and 1.784 for Mn, Cu, and V, respectively.
(30) Polyhedral volumes were calculated using the program VESTA based on the structural parameters in Table 2 ($MnCu_3V_4O_{12}$) and ref 7 ($MnVO_3$).

(31) Dilly, N. R.; Bauer, E. D.; Maple, M. B.; Dordevic, S.; Basov, D. N.; Freibert, F.; Darling, T. W.; Migliori, A.; Chakoumakos, B. C.; Sales, B. C. *Phys. Rev. B* **2000**, *61*, 4608.
(32) Qiu, L.; Swainson, I. P.; Nolas, G. S.; White, M. A. *Phys. Rev. B* **2004**, *70*, 035208.
(33) Yamaura, J.; Yonezawa, S.; Muraoka, Y.; Hiroi, Z. *J. Solid State Chem.* **2006**, *179*, 336.
(34) Shiraki, H.; Saito, T.; Azuma, M.; Shimakawa, Y. *J. Phys. Soc. Jpn.* **2008**, *77*, 064705.
(35) Braun, D. J.; Jeitschko. *J. Less-Common Met.* **1980**, *72*, 147.
(36) Evers, C. B. H.; Jeitschko, W.; Boonk, L.; Braun, D. J.; Ebel, T.; Scholz, U. D. J. *J. Alloys Compd.* **1995**, *224*, 184.
(37) Keppens, V.; Mandrus, D.; Sales, B. C.; Chakoumakos, B. C.; Dai, P.; Coldea, R.; Maple, M. B.; Gajewski, D. A.; Freeman, E. J.; Bennington, S. *Nature* **1998**, *395*, 876.
(38) Sales, B. C.; Mandrus, M.; Williams, R. K. *Science* **1996**, *272*, 1325.
(39) Goto, T.; Nemoto, Y.; Sakai, K.; Yamaguchi, T.; Akatsu, M.; Yanagisawa, T.; Hazama, H.; Onuki, K.; Sugawara, H.; Sato, H. *Phys. Rev. B* **2004**, *69*, 180511(R).
(40) Yanagisawa, T.; Ho, P. C.; Yuhasz, M.; Maple, M. B.; Yasumoto, Y.; Watanabe, H.; Nemoto, Y.; Goto, T. *J. Phys. Soc. Jpn.* **2008**, *77*, 074607.
(41) Ho, P.-C.; Yuhasz, M.; Butch, N. P.; Frederic, N. A.; Sayles, T. A.; Jeffries, J. R.; Maple, M. B.; Betts, J. B.; Lacerda, A. H.; Rogl, P.; Giester, G. *Phys. Rev. B* **2005**, *72*, 094410.
(42) Cao, D.; Bridges, F.; Bushart, S.; Bauer, E. D.; Maple, M. B. *Phys. Rev. B* **2003**, *67*, 180511(R).
(43) Qiu, L.; Swainson, I. P.; Nolas, G. S.; White, M. A. *Phys. Rev. B* **2004**, *70*, 035208.